

Keck spectroscopy of young and old star clusters in NGC 1023 ¹

Søren S. Larsen and Jean P. Brodie

UC Observatories / Lick Observatory, University of California, Santa Cruz, CA 95064, USA

soeren@ucolick.org and brodie@ucolick.org

Received _____; accepted _____

arXiv:astro-ph/0111542v1 28 Nov 2001

ABSTRACT

We present Keck/LRIS spectra for 11 old globular clusters in the S0-type galaxy NGC 1023 and 2 young blue clusters in the nearby companion NGC 1023A. Analysis of the spectra of 7 old clusters with sufficient S/N shows generally good agreement between spectroscopic and previous photometric metallicity estimates, but the integrated colors of two clusters are too blue for their spectroscopic metallicities. Although the cluster ages are not well constrained, they are most likely similar to those of Milky Way globular clusters and certainly older than ~ 5 Gyr. The brightest GC in the sample shows enhanced cyanogen, possibly indicating an abundance anomaly similar to that observed in some M31 globular clusters.

For the two blue clusters in NGC 1023A we estimate ages between 125 and 500 Myr, based on their strong Balmer lines. The total masses are about $8 \times 10^4 M_{\odot}$ and $6 \times 10^4 M_{\odot}$ for a Miller-Scalo IMF and $Z = 0.004$, making these objects similar to the young populous clusters in the Large Magellanic Cloud. It is suggested that the two young clusters might have formed during a period of enhanced star formation activity in NGC 1023A, stimulated by a close encounter with NGC 1023.

Subject headings: galaxies: star clusters — galaxies: individual (NGC 1023)

¹Based on data obtained at the W.M. Keck Observatory, which is operated as a scientific partnership among the California Institute of Technology, the University of California and the National Aeronautics and Space Administration.

1. Introduction

At a distance of around 10 Mpc (Ciardullo, Jacoby and Harris 1991), NGC 1023 is one of the nearest S0-type galaxies. It is included in the *Atlas of peculiar galaxies* (Arp 1966) because of a small companion galaxy, NGC 1023A, which may have suffered a recent close encounter with NGC 1023 itself (Sancisi et al. 1984). The companion galaxy is quite noticeably bluer than NGC 1023. Its integrated broad-band colors, $U - B = 0.0$ and $B - V = 0.7$ (Capaccioli et al. 1986) would imply a metallicity of $[\text{Fe}/\text{H}] = -1.7$ or less for an entirely old stellar population (Bruzual and Charlot 2001), or the galaxy might have experienced recent star formation activity. There are no traces of line emission in its spectrum (Capaccioli et al. 1986), indicating no current star formation, but stars might have formed until a few 100 Myr ago when any residual gas was stripped during a close encounter with NGC 1023. With an absolute B magnitude of $M_B = -15.7$ (Capaccioli et al. 1986), NGC 1023A is about one magnitude fainter than the Small Magellanic Cloud (de Vaucouleurs et al. 1991), but the ongoing star formation in the SMC presumably gives it a somewhat lower mass-to-light ratio than NGC 1023A so the two galaxies might have quite comparable masses.

Although globular clusters (GCs) are easily detectable at the distance of NGC 1023, its GC system has received surprisingly little attention. This might be related to the fact that NGC 1023 is located at a Galactic latitude of only -19 deg, causing serious contamination problems from foreground stars in ground-based studies. A recent study of GCs in NGC 1023 was carried out by Larsen and Brodie (2000) (LB2000), who detected 221 cluster candidates with a clearly bimodal color distribution on HST / WFPC2 images. Among the clusters identified by LB2000 were a number of red objects, which were generally fainter and had larger effective radii than normal GCs. In this paper we discuss new spectroscopic data for normal compact globular clusters in NGC 1023 and for two young

clusters in the companion galaxy, NGC 1023A.

2. Observations

Objects to be observed with the LRIS spectrograph (Oke et al. 1995) on the Keck I telescope were picked from the list of GC candidates identified by LB2000. Additional objects to fill up the slitmask, including two blue objects in NGC 1023A, were selected from ground-based CCD images from the 1.2 m telescope at F. L. Whipple observatory on Mount Hopkins, Arizona, kindly provided by P. Barmby. The Keck spectra were obtained in February 2000, using 1'' slitlets and a 600 lines/mm grating blazed at 5000 Å. This provides a spectral resolution of about 6 Å and a scale of 1.28Å per pixel. The spectra typically covered the region 3900 Å – 6300 Å, but the limits varied by a few 100 Å from one spectrum to another. Altogether the slitmask included 20 science objects, of which 10 were selected from the LB2000 WFPC2 images. The total integration time was 9300 sec, split into 6 individual exposures. Flux standards from Massey et al. (1988) (PG0838+546 and PG0939+262) and 4 radial velocity standard stars (HR1805, HR3905, HD37251 and HD52071) were observed through a 1'' longslit. HR1805 and HR3905 were also observed by Worthey et al. (1994) in the Lick/IDS system, making them suitable for a consistency check of our own spectroscopy.

The multislit spectra were extracted from the individual images using the custom-designed REDUX package, written by A. Phillips. REDUX automatically detects each object spectrum and subtracts the sky background, based on information in the files that were originally used for designing the slitmasks. The wavelength solution was obtained by REDUX from exposures of arc spectra through a special calibration slitmask, with corrections to the wavelength zero-point from night sky lines. Co-addition of the individual integrations was also performed by REDUX. The flux- and radial velocity

standards were reduced using standard tools in the IRAF SPECRED package², and the flux calibrations were then applied to the multislit spectra. Radial velocities were obtained by cross-correlation of the object spectra with the spectra of the four radial velocity standards, using the FXCOR task in the RV package in IRAF.

Basic data for the science objects are listed in Table 1. The first column in the table is an object identifier and the second column indicates whether the object was selected from the ground-based or WFPC2 data. The following columns list the 2000.0 coordinates and V, I photometry (uncorrected for reddening). Column 7 gives the mean heliocentric radial velocity from the four individual measurements and the standard error on the mean value. Finally, column 8 lists the signal-to-noise per pixel in the dispersion direction of each spectrum in the region 4900Å– 5100Å.

The radial velocity of NGC 1023 is listed as 601 ± 11 km/sec in the RC3 catalogue, while Capaccioli et al. (1986) find a somewhat higher radial velocity of 742 ± 30 km s⁻¹ for NGC 1023A. Many of the objects selected on the ground-based images were near the detection limit (as is evident from the large photometric errors) and some are probably spurious detections (n1023-7, n1023-12, n1023-23). Others did not reveal a clear cross-correlation signal anywhere near the NGC 1023 radial velocity (n1023-18, n1023-20) and are presumably background galaxies. n1023-18 shows broad emission lines characteristic of quasars, corresponding to the CIV and CIII] lines at rest wavelengths 1549 Å and 1909 Å, redshifted to $z = 2.15$ (Fig. 1). n1023-24 is probably a foreground star. Two objects are good GC candidates (n1023-13 and n1023-25), and we call particular attention to object n1023-13 (Fig. 1) whose apparent V band magnitude corresponds to an absolute

²IRAF is distributed by the National Optical Astronomical Observatories, which are operated by the Association of Universities for Research in Astronomy, Inc. under contract with the National Science Foundation

magnitude of $M_V = -10.8$ at the distance of NGC 1023. This cluster, discussed in detail in Larsen (2001), is about half a magnitude brighter than the brightest globular cluster in the Milky Way, ω Centauri (Harris 1996). The two blue objects in NGC 1023A, n1023-3 and n1023-4, have strong Balmer lines, indicating the presence of A-type stars, and radial velocities consistent with the NGC 1023 system and with NGC 1023A in particular. Of the HST-selected objects, n1023-15 is presumably a background galaxy, but the remaining 9 objects are good GC candidates. Thus, our data include 11 old globular clusters in NGC 1023 and 2 young objects in NGC 1023A. The mean radial velocity of the whole sample is 597 km/s with a dispersion of ± 154 km/s, or 573 ± 155 km/s if the two young clusters are excluded, in nice agreement with the radial velocity of NGC 1023 quoted above.

3. Spectrophotometric analysis of abundances and ages

Although the metallicities of globular clusters are generally believed to correlate with their broad-band colors, a spectroscopic analysis provides more detailed information on possible anomalies and/or age differences. An empirical calibration of various spectrophotometric indices as a function of metallicity was published by Brodie and Huchra (1990, hereafter BH90), and more recently Lick/IDS indices for stellar populations of various ages and metallicities have been modeled by e.g. Worthey (1994), Bruzual and Charlot (2001), C. Maraston and others.

The BH90 metallicity calibration is based on a number of metallicity-sensitive spectrophotometric indices, each of which provides an estimate of the metallicity. A weighted mean of these individual measurements then provides the final spectroscopic metallicity estimate of the cluster, where the appropriate weights are determined from the random errors on the index measurements as well as from the inherent uncertainty in the metallicity derived from a given index. The latter contribution is given by the

“figure of merit” for each index, as defined by BH90. Even though we will often label these estimates by $[\text{Fe}/\text{H}]$, it should be emphasized that the metallicity calibrators really measure a variety of different elements, including C, N, Mg and Fe. In our treatment of the errors we adopt one modification from the BH90 prescription, whose equation (22) gives the weighted dispersion of the individual $[\text{Fe}/\text{H}]$ measurements rather than the uncertainty on the weighted mean. Thus, we multiply by a factor $(\sum W_j - 1)^{-1/2}$ so that our error on the combined $[\text{Fe}/\text{H}]$ estimate, σ_W , becomes

$$\sigma_W = \left[\frac{\sum W_j ([\text{Fe}/\text{H}]_I - [\text{Fe}/\text{H}]_W)^2}{(\sum W_j) (\sum W_j - 1)} \right]^{1/2} \quad (1)$$

where W_j are the weights (normalized to the range $0 \leq W_j \leq 1$) and $[\text{Fe}/\text{H}]_I$ and $[\text{Fe}/\text{H}]_W$ are the individual and weighted mean metallicity estimates.

Spectrophotometric indices are generally based on a central bandpass covering the feature of interest and two bandpasses on either side of the feature bandpass which define a “pseudo-continuum”. Several variants of the exact prescription exist in the literature, mainly differing in the way the fluxes in the continuum bandpasses are interpolated to the feature bandpass (Burstein et al. 1984; Worthey et al. 1994, BH90). In practice, the definitions by Burstein et al. (1984) and Worthey et al. (1994) usually give virtually identical results, while indices computed according to BH90 can be slightly different, especially if the continuum passbands are located asymmetrically with respect to the feature bandpass and the spectrum has a significant slope.

3.1. Metallicities

We derived spectroscopic metallicities for old globular clusters with $S/N > 5$ using the calibration in BH90. Indices were measured according to their prescription after correction for radial velocities as listed in Table 1. If instead the Burstein et al. (1984) or Worthey et

al. (1994) definitions were used, we found a slight decrease in the $[\text{Fe}/\text{H}]$ values by about 0.02 dex, with most of the difference coming from the Fe5270 index. Thus, it is clear that the exact prescription used for measuring the indices has only a very weak effect on the resulting metallicities. As a check, we also compared our index measuring software with the SBANDS task in IRAF (which uses the Burstein et al. definition) and got identical values when using that same definition.

Each of the individual metallicity estimates, as well as the mean values, are given in Table 2 for the 7 old clusters with $S/N > 5$. Of these clusters, 6 belong to the “blue” peak in the color distribution as defined by LB2000 $[(V-I)_0 < 1.05]$ and one (n1023-25) belongs to the “red” peak. Because none of the spectra reached sufficiently far into the blue, the BH90 Δ index could not be measured for any of the clusters and has therefore not been included in the Table. Furthermore, we have excluded the NaD index because of the strong NaD skylines, which at best add large amounts of noise to measurements of this index and at worst may cause systematic errors. For comparison, we also list metallicities derived from the reddening-corrected $V-I$ colors, using the calibration in Kissler-Patig et al. (1998) and adopting a foreground extinction of $A_B = 0.26$ (Schlegel et al. 1998). The uncertainties on these photometric metallicities only include the random errors due to the photometry, while no systematic errors in the calibrations etc. have been taken into account.

Although most of the individual metallicity estimators are compatible with the average values within the errors for any given cluster, it may be worth noting that the measurements based on the Fe5270 index tend to give higher metallicities than the other indices. Typically, the $[\text{Fe}/\text{H}]$ values based on the Fe5270 index fall about 0.5 dex above the mean values. In Figure 2 we compare the spectroscopic and photometric metallicities. There is generally fair agreement between the two metallicity estimates, although we note the presence of two outliers (n1023-14 and n1023-16) for which the spectroscopic measurements give

significantly higher metallicities than the photometric ones. The reason for this is not clear, but from Table 2 the discrepancy does not appear to be driven by any individual index, except for the high metallicity from the Fe5270 index which is common to all clusters. In fact, *all* of the individual metallicity estimators give higher values than the photometric estimate for these two objects. We also measured “pseudo-colors” for the clusters on the spectra at 4700 Å and 5700 Å in 500 Å windows (Table 3), confirming that n1023-14 and n1023-16 have rather blue colors for their metallicities.

The data used by BH90 came from a variety of instruments with different spectral resolutions, ranging from about 5 Å (AAT and MMT) to 12 Å (Lick). To test how the results depend on the spectral resolution, we smoothed our data with an 8 pixels (10 Å) wide Gaussian kernel to simulate the 12 Å resolution of the lowest resolution spectra used by BH90 and redid the metallicity measurements. Such smoothing typically decreased the metallicities by ~ 0.1 dex. Since only a fraction of the BH90 data were observed at 12 Å resolution and the rest were observed at a resolution quite similar to ours, systematic errors on our mean metallicity estimates due to resolution effects should be smaller than 0.1 dex.

Burstein et al. (1984) and Brodie and Huchra (1991) noted that many GCs in M31 have enhanced CNR indices compared to Galactic globulars of the same metallicity. Table 4 lists a number of indices for the 7 brightest old GCs in NGC 1023, and in Fig. 3 we show the CNR indices versus [Fe/H]. The polygon represents the approximate region of the diagram populated by Galactic globulars, according to Brodie and Huchra (1991). We note that two clusters (n1023-13 and n1023-14) do seem to have enhanced CNR indices, although this may only be significant for n1023-13 due to the larger errors on the data for n1023-14. For the remaining spectra the errors are too large to put strong constraints on any anomalies although most of them seem to be compatible with the Milky Way data.

3.2. Comparison with population synthesis models

Age differences between clusters would manifest themselves most strongly in the Balmer lines. Beyond a few hundred Myrs the strength of the Balmer lines decreases as a function of age, as the main sequence turn-off shifts towards cooler temperatures. However, it is important to note that the appearance of blue horizontal-branch stars in metal-poor populations around 10 Gyr can reverse this trend, potentially making the Balmer lines less useful as age indicators in very old, metal-poor populations (Maraston & Thomas 2000). Also, many population synthesis models suffer from uncertainties in the modeling of AGB stars which can have a significant effect on the Balmer indices (Schiavon et al. 2002). With those precautions in mind, we compare our data with model predictions from Bruzual and Charlot (2001) (BC2001) in the following.

There are a few instrumental effects that need to be considered when comparing our measurements with the BC2001 models, which use line indices based on the Worthey et al. (1994) fitting functions. First, the Lick/IDS spectra were not flux calibrated and second, our $\sim 6 \text{ \AA}$ resolution is higher than that of the Lick/IDS spectra. In order to test how sensitive our measured indices are to these effects, Table 5 lists measurements of a selection of Lick/IDS indices on flux-calibrated spectra of the two Lick standards HR1805 and HR3905, as well as on unfluxed spectra and spectra smoothed with a 5 pixels wide Gaussian kernel to simulate the lower Lick/IDS resolution. Generally, flux calibration only affects the equivalent widths by a few times 0.01 \AA , in most cases much smaller than the random measurement errors. This has also been documented by other authors (e.g. Faber et al. 1985; Kissler-Patig et al. 1998), but see Beasley et al. (2000) for some cautionary notes. However, the smoothing does have a significant effect on the results in some cases. The EWs measured on the unsmoothed data are generally too high by several times 0.1 \AA compared to the Worthey et al. standard values, while smoothing of the data clearly results

in better agreement. We therefore decided to smooth all the science spectra with a 5 pixels Gaussian kernel before measuring Lick / IDS indices.

Selected Lick/IDS indices for the NGC 1023 clusters are listed in Table 6. The last row gives the mean indices for all of the 6 metal-poor old clusters, i.e. excluding n1023-3, n1023-4 and n1023-25. In Figure 4 and 5 we compare the Fe5270, Mg2 and $H\beta$ measurements in Table 6 with the BC2001 models. The mean values from Table 6 are indicated with * symbols. From Figure 4 and 5, most clusters are at least several Gyrs old, except for n1023-3 and n1023-4 whose very strong Balmer lines imply ages less than 500 Myr (see Section 4). The combined datapoint falls near the 10/15 Gyr isochrones in both plots, and between the $[Fe/H] = -0.7$ and -1.7 lines, in agreement with the metallicities derived from the BH90 calibration. However, the separation between the 5, 10 and 15 Gyr isochrones in these diagrams is comparable to the errors even for the combined data and the theoretical 10 Gyr and 15 Gyr lines actually *cross each other* at $[Fe/H] \sim -1$. Both Fig. 4 and Fig. 5 formally indicate an age of ~ 1 Gyr and above solar metallicity for the faint cluster n1023-25, but the error bars are large and it seems premature to conclude that this cluster is truly young. It would be interesting to obtain high S/N spectra of additional metal-rich GCs in NGC 1023 and look for age differences between metal-poor and metal-rich clusters.

To summarize, the spectroscopy generally confirms the photometric metallicity estimates, but we find that two clusters have significantly higher spectroscopic metallicities than would be expected from their integrated colors. We note that the bright cluster n1023-13 shows a possible enhancement in the CNR index, similar to that observed in some M31 clusters. Most of the GCs appear to be old ($\gtrsim 5$ Gyr) and have ages consistent with those of Milky Way globulars, but the ages are not well constrained.

4. The two blue objects in NGC 1023A

Davies and Kinman (1984) noted a number of faint point sources in NGC 1023A, near the detection limit on their photographic plates, and suggested that these might be supergiant stars. The ground-based CCD images from which we selected our GC candidates for Keck spectroscopy clearly showed two blue sources superimposed on NGC 1023A, which we decided to include in our sample.

The spectra of these two objects, n1023-3 and n1023-4 turned out to be nearly identical and only one of them is shown in Figure 1. The most striking features of the spectra are the very strong Balmer lines, an obvious indication that these are young objects dominated by A-type stars, and thus with ages of no more than a few times 10^8 years. The radial velocities are compatible with NGC 1023 membership, and actually favor association with NGC 1023A. After correction for reddening, the ground-based photometry indicates $(B-V)_0 = 0.25 \pm 0.06$ and 0.36 ± 0.04 , $(V-I)_0 = 0.62 \pm 0.08$ and 0.60 ± 0.04 , and $M_V = -9.25 \pm 0.05$ and -9.54 ± 0.03 for the two objects. Only stars with masses above $35 M_\odot$ reach such high luminosities, and have lifetimes less than 5 Myr (Bertelli et al. 1994; Girardi et al. 2000). Star formation activity that recent would still be easily detectable as $H\alpha$ emission, which is clearly incompatible with the observations – notwithstanding the fact that it would be highly unlikely to find two isolated stars that massive. Thus, the two blue “central condensations” in NGC 1023 are most likely young star clusters. Unfortunately, they are not included in any HST images and the available ground-based images have insufficient resolution and S/N to tell whether or not they are spatially extended.

4.1. Spectroscopic ages

Fig. 6 shows BC2001 model predictions for the evolution of the Lick/IDS $H\beta$ index as a function of age for three different metallicities: $Z = 0.02$ (solar), $Z = 0.008$ and $Z = 0.004$. The plot also includes model predictions by C. Maraston (private comm.) for solar metallicity. The Maraston models are also available for sub-solar metallicities, but these have been omitted here for clarity. Equivalent widths of the $H\beta$ line measured for the two blue objects in NGC 1023A are indicated by the hatched areas. From Figure 4 and Figure 5 the two objects appear to have subsolar metallicities, as expected if they formed in a stellar environment similar to that of the SMC, but the measurement and model uncertainties are too large to provide strong constraints on the exact metallicities.

As can be seen from Fig. 6, age determinations based on Balmer lines alone are ambiguous, because the predicted equivalent widths reach a maximum at a few times 10^8 years. For solar metallicity ($Z = 0.02$), comparison with the BC2001 models suggests cluster ages around 125 Myr or around 300 Myr, but for $Z = 0.004$ (similar to that of the young stellar population in the SMC) the ages could be as high as ~ 500 Myr. The best match to the Maraston models is obtained at an age around 200–300 Myr.

The Worthey et al. (1994) fitting functions, used by both the BC2001 and the Maraston models, were tailored primarily for studies of old stellar populations in early-type galaxies, and may produce less reliable results for younger stellar populations. An alternative set of broader indices, tailored for young stellar populations, was introduced by Brodie et al. (1998). We hereafter refer to these indices as B98 indices. In Fig. 7 we compare B98 ($H\beta$, $H\gamma$, $H\delta$) equivalent widths with model predictions based on the spectral energy distributions (SEDs) supplied with the Bruzual and Charlot (2001) models. B98 indices computed by C. Maraston (private comm.) produce essentially the same results. Figure 7 also shows the model predictions for $B - V$ colors and the ground-based measurements.

Again, Figure 7 shows that both clusters are young objects with ages on the order of 300 Myr, but note that nearly all the Balmer line indices are *stronger* than the maximum values predicted by the models. A similar effect was observed by Brodie et al. (1998) for young clusters in NGC 1275. They suggested that the unusually strong Balmer lines might be due to a skewed or truncated stellar IMF, and found that the observed Balmer line EWs were better reproduced by models with a lack of stars below $\sim 2M_{\odot}$. Although Brodie et al. (1998) only adopted the truncated IMF models as the best available approximation to a flatter IMF, not necessarily implying a complete lack of low-mass stars in the real clusters, it is clear that the IMF would have to be dramatically different from the “standard” Salpeter slope in order to produce significant changes in the observed EWs of spectral lines. Using BC2001 models computed for a Miller-Scalo IMF instead of Salpeter, for example, has virtually no impact on the predicted EWs.

In conclusion, the integrated spectra of young stellar populations clearly need to be better understood. With current models we cannot constrain the age of the two blue objects in NGC 1023A to better than somewhere between 125 and 500 Myr. Part of the uncertainty is due to the behavior of Balmer line strengths as a function of age, but it is also worth noting that different models and index definitions can provide significantly different results. However, we note that the estimated cluster ages are compatible with the clusters having formed during the last close encounter between NGC 1023 and NGC 1023A.

4.2. Masses

Because of the uncertain ages and other factors, estimates of the total cluster masses are also inherently uncertain. However, we can make some crude estimates: For a Miller-Scalo IMF and an age of 300 Myr, the BC2001 models predict a luminosity per solar mass of $M_V(1M_{\odot}) = 2.74$ for $Z = 0.004$. For $Z = 0.02$ the models predict $M_V(1M_{\odot}) = 2.95$. If

we adopt an uncertainty of ± 100 Myr for the ages (which may be somewhat optimistic, cf. the discussion in the previous section) then the corresponding uncertainty on the V band M/L ratio is about ± 0.3 mag. Considering the uncertainty on metallicity, a more realistic error estimate on the M/L ratio may be at least 0.5 mag. With absolute V band magnitudes of -9.54 and -9.25 the masses of the two clusters then become $8.2 \times 10^4 M_{\odot}$ and $6.2 \times 10^4 M_{\odot}$, with an uncertainty of about $\pm 50\%$. For a Salpeter IMF extending down to $0.1 M_{\odot}$ the masses are roughly a factor of two higher than those based on the Miller-Scalo IMF, i.e. $1.8 \times 10^5 M_{\odot}$ and $1.3 \times 10^5 M_{\odot}$ for the two clusters. For a truncated IMF the masses would be even smaller than for the Miller-Scalo IMF. However, it is clear that the two blue clusters in NGC 1023A are fairly massive, and they may be quite similar to young “populous” clusters such as NGC 1866 in the LMC (Hodge 1961).

4.3. Are the young blue clusters in NGC 1023A related to the “faint fuzzies” in NGC 1023?

LB2000 discovered a number of peculiar faint, extended objects in NGC 1023, thought to be stellar clusters associated with the disk of the galaxy. These clusters have about the same $V-I$ color as the metal-rich “normal” globular clusters in NGC 1023, but are generally fainter and have larger sizes. Most of them have effective radii of ~ 10 pc and absolute visual magnitudes fainter than $M_V = -7$. While their origin remains unknown, one possibility is that they might have been accreted from dwarf galaxies similar to NGC 1023A. Some support for this idea is provided by the presence of an HI-ring around NGC 1023, hinting at encounters in the system earlier in its history (Capaccioli et al. 1986). It is thus natural to ask how the two blue objects in NGC 1023A will evolve with time.

Assuming that the two blue objects currently have ages of 300 Myr, they will fade by ~ 1 magnitude by the time they are 1 Gyr old and by about 3.5 mag when they reach an

age of 10 Gyr. Thus, they will be in the magnitude range spanned by the “faint fuzzies” several Gyr from now, provided they remain bound. This by itself, of course, does not imply that the faint extended clusters in NGC 1023 originated in dwarf galaxies similar to NGC 1023A, but it would be highly desirable to check the sizes of the two blue clusters with high-resolution imaging.

5. Summary and conclusions

We have presented Keck spectroscopy for 11 old globular clusters in the nearby S0-type galaxy NGC 1023 and 2 young clusters in its companion galaxy, NGC 1023A. Out of 10 objects from Larsen and Brodie (2000), 9 are confirmed to be globular clusters in NGC 1023 and in addition we have identified 2 new globular clusters, one of which is very luminous with $M_V \approx -10.8$. Most of the spectra have rather poor S/N but 7 are good enough to allow analysis of metallicities. Two of these clusters have higher metallicities than predicted by their broad-band colors. We have looked for abundance anomalies and find that most clusters show no detectable anomalies, although the bright cluster n1023-13 may show cyanogen enhancements similar to those observed in M31 globular clusters (Burstein et al. 1984; Brodie and Huchra 1991). Most of the clusters appear to have high ages consistent with Milky Way globulars, but the errors are large and it would be highly desirable to check possible age differences between the metal-poor and metal-rich populations with more spectra of metal-rich GCs in NGC 1023.

Two blue objects in NGC 1023A are young star clusters with ages around 300 Myr, but with a possible range between 125 and 500 Myr. Their integrated V band magnitudes are $M_V = -9.6$ and $M_V = -9.3$. The total masses are about $8 \times 10^4 M_\odot$ and $6 \times 10^4 M_\odot$ for a Miller-Scalo IMF and SMC-like metallicity, making these clusters similar to young populous clusters in the LMC such as NGC 1866. Since NGC 1023 and NGC 1023A

may have undergone a close encounter at about the same time the two blue clusters in NGC 1023A were formed, it is tempting to speculate that the clusters formed during a period of enhanced star formation activity, stimulated by the encounter.

We are grateful to Pauline Barmby for providing us with her ground-based CCD images of NGC 1023 and to Markus Kissler-Patig for helpful comments on an earlier version of this manuscript. We also thank John Huchra for useful discussions and the anonymous referee for comments which helped improve the manuscript. This work was supported by National Science Foundation grant number AST9900732.

REFERENCES

- Arp, H. C. 1966, *ApJS*, 14, 1
- Beasley, M. A., Sharples, R. M., Bridges, T. J., Hanes, D. A., Zepf, S. E., Ashman, K. M., & Geisler, D. 2000, *MNRAS*, 318, 1249
- Bertelli, G., Bressan, A., Chiosi, C., Fagotto, F., & Nasi, E. 1994, *A&AS*, 106, 275
- Brodie, J. P. and Hanes, D. A., 1986, *ApJ*, 300, 258
- Brodie, J. P. and Huchra, J. P. 1990, *AJ*, 362, 503
- Brodie, J. P., Schroder, L. L., Huchra, J. P., Phillips, A. C., Kissler-Patig, M., & Forbes, D. A. 1998, *AJ*, 116, 691
- Brodie, J. P. and Huchra, J. P. 1991, *AJ*, 379, 157
- Bruzual, G. A. and Charlot, S. 2001, in preparation
- Burstein, D., Faber, S. M., Gaskell, C. M., & Krumm, N. 1984, *ApJ*, 287, 586
- Capaccioli, M., Lorenz, H., and Afanasjev, V. L. 1986, *A&A*, 169, 54
- Ciardullo, R., Jacoby, G. H., and Harris, W. E. 1991, *ApJ*, 383, 487
- Davies, R. D., and Kinman, T. D. 1984, *MNRAS*, 207, 173
- de Vaucouleurs, G., de Vaucouleurs, A., Corwin Jr., H. G. et al. 1991, Third Reference Catalogue of Bright Galaxies, Version 3.9 (RC3)
- Faber, S. M., Friel, E. D., Burstein, D., & Gaskell, C. M. 1985, *ApJS*, 57, 711
- Girardi, L., Bressan, A., Bertelli, G., & Chiosi, C. 2000, *A&AS*, 141, 371
- Harris, W. E. 1996, *AJ*, 112, 1487

- Hodge, P. W. 1961, ApJ, 133, 413
- Kissler-Patig, M., Brodie, J. P., Schroder, L. et al., 1998, AJ, 115, 105
- Larsen, S. S. 2001, AJ, 122, 1782
- Larsen, S. S., and Brodie, J. P., 2000, AJ, 120, 2938 (LB2000)
- Maraston, C. & Thomas, D. 2000, ApJ, 541, 126
- Massey, P., Strobel, K., Barnes, J. V., & Anderson, E. 1988, ApJ, 328, 315
- Oke, J. B. Cohen, J. G., Carr, M. et al. 1995, PASP, 107, 375
- Sancisi, R., van Woerden, H., Davies, R. D., and Hart, L. 1984, MNRAS, 210, 497
- Schiavon, R. P., Faber, S. M., Rose, J. A., Castilho, B. V., 2002, AJ, submitted
(astro-ph/0109365)
- Schlegel, D. J., Finkbeiner, D. P., and Davis, M. 1998, ApJ, 500, 525
- Worthey, G. 1994, ApJS, 95, 107
- Worthey, G., Faber, S. M., González, J. J., and Burstein, D. 1994, ApJS, 94, 687

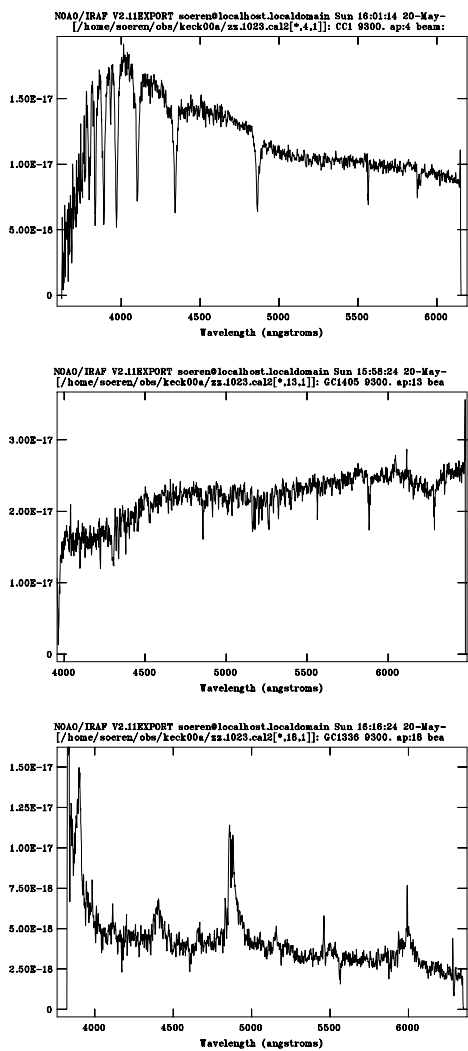


Fig. 1.— (a) One of the blue objects in NGC 1023A (n1023-4). Note the very strong Balmer lines. (b) The bright globular cluster (n1023-13). (c) Object n1023-18, showing broad emission lines corresponding to CIV (1549 Å) and CIII] (1909 Å) redshifted to $z = 2.15$ and thus presumably a quasar. All spectra have been smoothed with a 3 pixels wide boxcar filter.

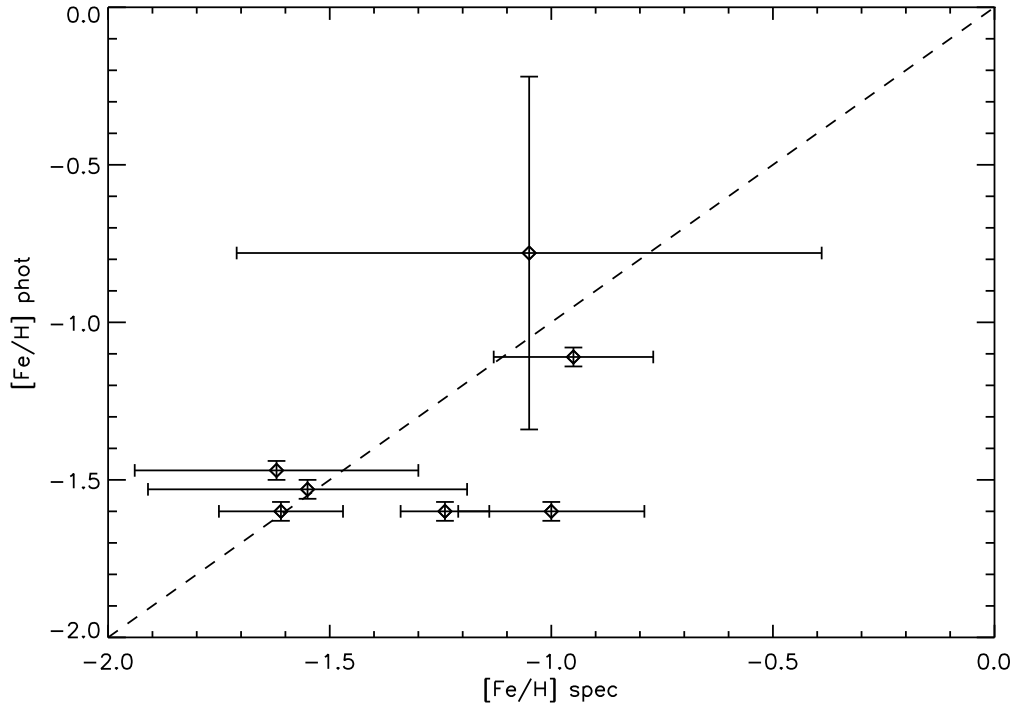


Fig. 2.— Comparison of average spectroscopic versus photometric metallicities. The dashed line represents a 1:1 relation.

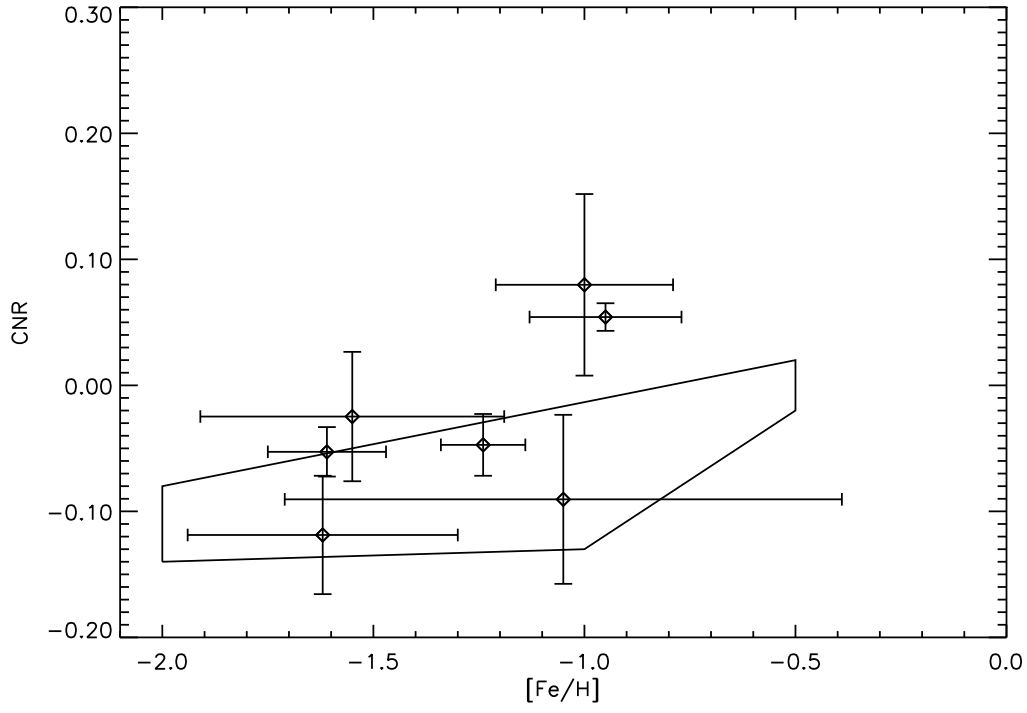


Fig. 3.— CNR indices as a function of metallicity. The polygons outline the part of the diagram populated by Milky Way globulars (from Brodie & Huchra 1991).

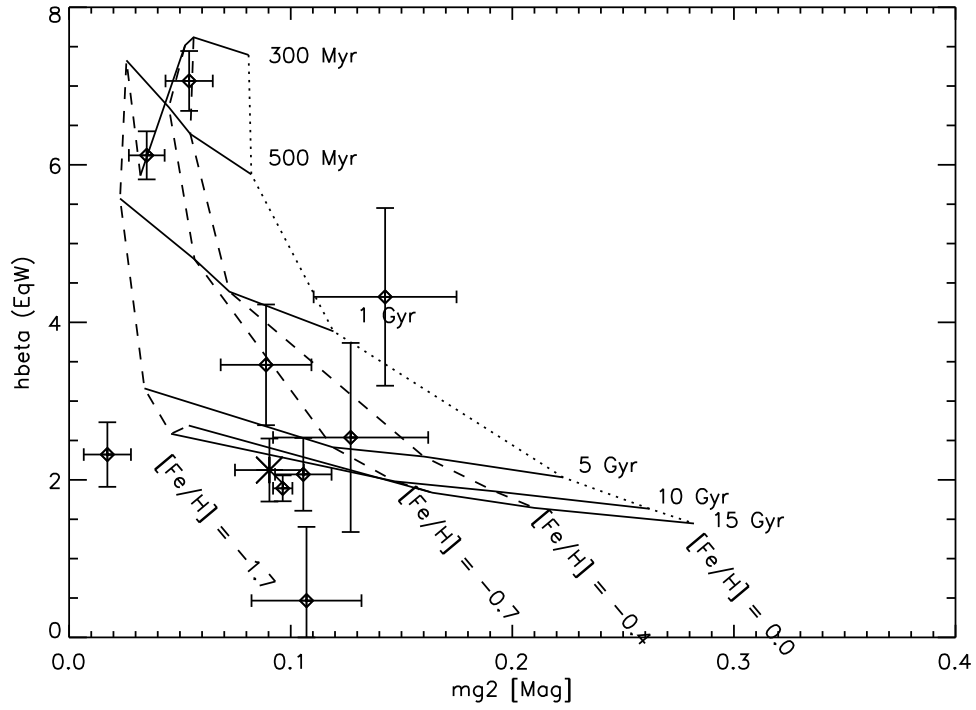


Fig. 4.— Lick/IDS $H\beta$ vs. Mg_2 indices, compared to Bruzual and Charlot (2001) population synthesis models. The asterisk (*) marks the combined data for the 6 old metal-poor GCs.

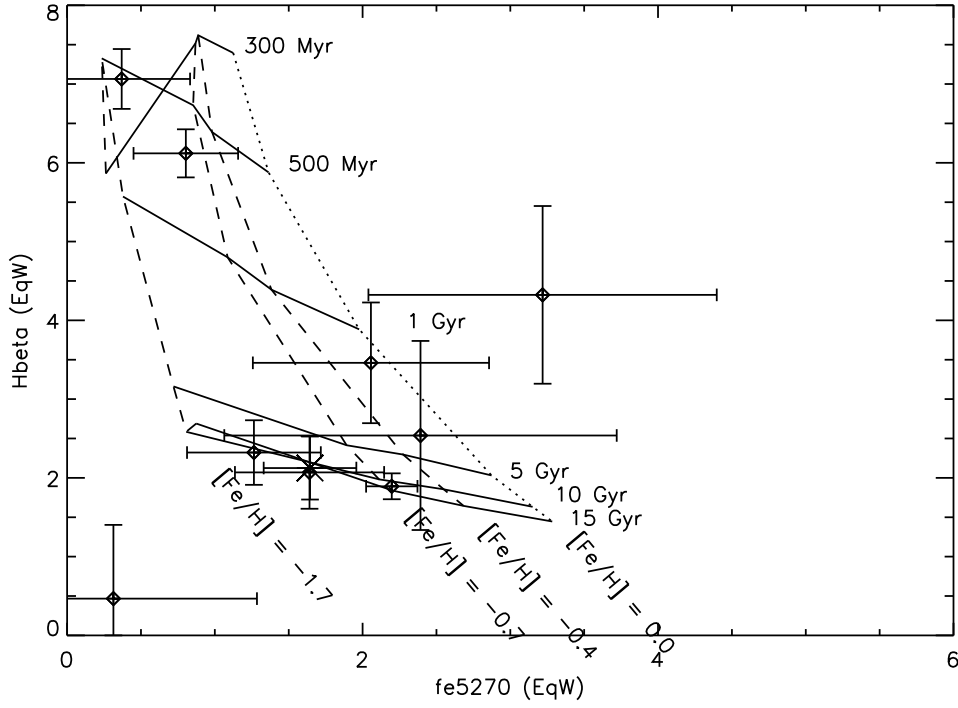


Fig. 5.— Lick/IDS $H\beta$ vs. Fe5270 indices, compared to Bruzual and Charlot (2001) population synthesis models.

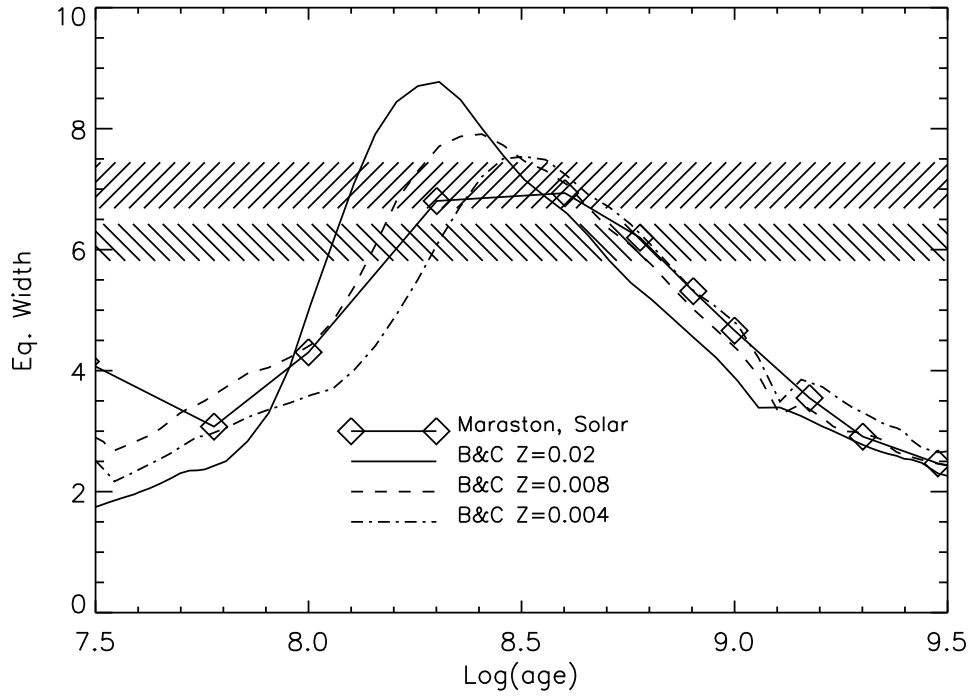


Fig. 6.— Models for the Lick/IDS $H\beta$ index as a function of age, compared to the measured values for the two blue objects in NGC 1023A, n1023-3 and n1023-4. The hatched areas indicate the measured values and their uncertainties.

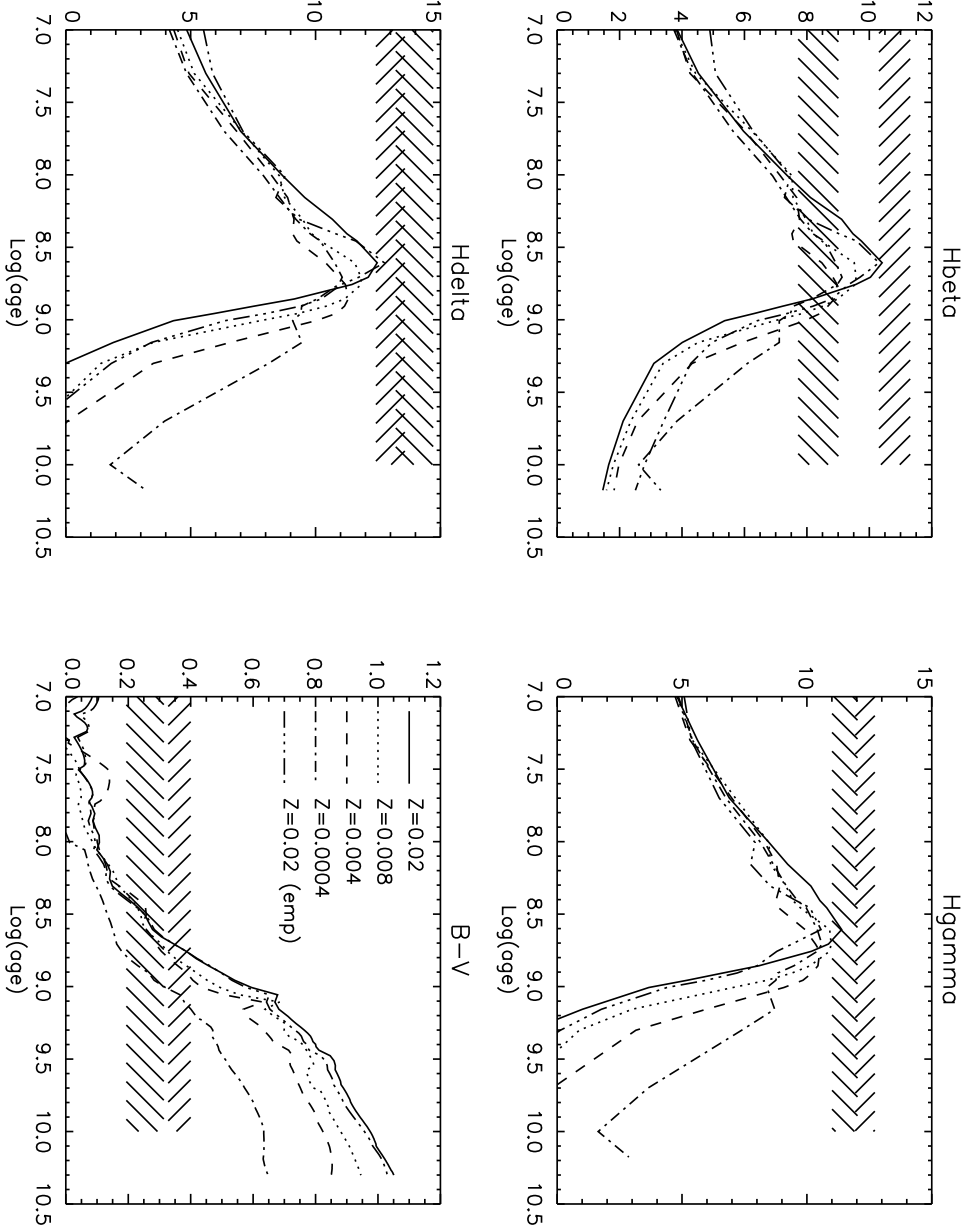


Fig. 7.— Balmer line equivalent widths and $B-V$ color for the two blue objects in NGC 1023A, compared to predictions based on Bruzual & Charlot (2001) models. The various curves in each diagram represent different metallicities.

Table 1. Spectroscopic data for globular cluster candidates in NGC 1023

Object	Obs	RA(2000)	DEC(2000)	V	$V-I$	RV (km/s)	S/N
n1023-3	Ground	2:40:37.91	39:03:30.8	20.9 ± 0.05	0.72 ± 0.08	729 ± 18	21.8
n1023-4	Ground	2:40:36.98	39:03:27.4	20.6 ± 0.03	0.70 ± 0.04	736 ± 17	28.1
n1023-7	Ground	2:40:33.14	39:03:48.5	22.4 ± 0.29	1.13 ± 0.42	-	0.1
n1023-8	HST	2:40:32.27	39:04:26.3	22.07 ± 0.01	1.21 ± 0.01	628 ± 37	2.4
n1023-9	HST	2:40:31.29	39:03:33.0	22.02 ± 0.01	0.98 ± 0.01	369 ± 53	3.5
n1023-10	HST	2:40:30.58	39:03:33.2	21.91 ± 0.01	1.26 ± 0.01	812 ± 32	2.8
n1023-11	HST	2:40:30.57	39:04:39.0	22.22 ± 0.01	1.27 ± 0.01	584 ± 195	3.5
n1023-12	Ground	2:40:29.69	39:04:21.3	21.4 ± 0.25	0.65 ± 0.53	-	0.0
n1023-13	Ground*	2:40:27.84	39:04:40.2	19.39 ± 0.01	1.14 ± 0.01	353 ± 17	53.0
n1023-14	HST	2:40:24.61	39:04:29.8	22.00 ± 0.01	0.99 ± 0.01	722 ± 22	7.0
n1023-15	HST	2:40:23.95	39:04:48.7	21.59 ± 0.01	1.30 ± 0.01	-	11.2
n1023-16	HST	2:40:21.02	39:04:26.3	21.13 ± 0.01	0.99 ± 0.01	736 ± 18	19.0
n1023-17	HST	2:40:20.56	39:04:57.0	21.44 ± 0.01	1.01 ± 0.01	449 ± 25	11.4
n1023-18	Ground	2:40:19.62	39:04:24.6	21.3 ± 0.14	1.14 ± 0.20	$z = 2.15$	12.6
n1023-19	HST	2:40:18.96	39:04:32.9	21.83 ± 0.01	1.03 ± 0.01	603 ± 17	9.6
n1023-20	Ground	2:40:17.57	39:03:58.4	22.4 ± 0.64	1.71 ± 0.75	-	2.5
n1023-21	HST	2:40:16.83	39:03:51.4	20.94 ± 0.01	0.99 ± 0.01	625 ± 20	20.5
n1023-23	Ground	2:40:14.75	39:04:10.2	21.9 ± 0.17	0.53 ± 0.39	-	0.0
n1023-24	Ground	2:40:13.39	39:03:45.7	21.2 ± 0.08	0.94 ± 0.13	-125 ± 16	15.3
n1023-25	Ground	2:40:12.99	39:04:29.1	22.3 ± 0.13	1.24 ± 0.17	421 ± 29	7.3

Note. — RV = heliocentric radial velocity, V = visual magnitude. The S/N column gives the average Signal-to-Noise in the region 4900Å– 5100 Å. * photometry from HST image in 0".5 aperture

Table 2. Metallicity estimates for globular clusters with spectra with $S/N > 5$.

Uncertainties have been estimated as described in BH90.

Object	Individual [Fe/H] estimators							[Fe/H] (sp)	[Fe/H] (phot)
	Mg2	MgH	Gband	CNB	Fe5270	CNR	H+K		
n1023-13	-1.20 ± 0.34	-1.42 ± 0.48	-0.73 ± 0.34	–	-0.56 ± 0.62	-0.79 ± 0.46	–	-0.95 ± 0.18	-1.11 ± 0.03
n1023-14	-0.95 ± 0.49	-1.53 ± 0.74	-1.37 ± 0.87	–	-0.55 ± 1.00	-0.61 ± 0.69	-0.95 ± 1.06	-1.00 ± 0.21	-1.60 ± 0.03
n1023-16	-1.05 ± 0.36	-1.24 ± 0.52	-1.31 ± 0.45	–	-0.98 ± 0.68	-1.54 ± 0.49	-1.35 ± 0.58	-1.24 ± 0.10	-1.60 ± 0.03
n1023-17	-1.17 ± 0.40	-2.22 ± 0.58	-2.29 ± 0.72	–	-0.82 ± 0.77	-1.37 ± 0.59	–	-1.55 ± 0.36	-1.53 ± 0.03
n1023-19	-1.09 ± 0.42	-1.20 ± 0.63	-2.46 ± 0.73	–	-2.11 ± 0.82	-2.06 ± 0.57	-1.11 ± 0.93	-1.62 ± 0.32	-1.47 ± 0.03
n1023-21	-2.08 ± 0.35	-1.31 ± 0.51	-1.69 ± 0.41	-1.76 ± 0.46	-1.16 ± 0.66	-1.58 ± 0.47	-1.36 ± 0.53	-1.61 ± 0.14	-1.60 ± 0.03
n1023-25	-0.80 ± 0.47	-0.32 ± 0.72	-0.96 ± 1.02	–	0.59 ± 0.95	-1.86 ± 0.67	-3.35 ± 1.07	-1.05 ± 0.66	-0.78 ± 0.56

Table 3. Comparison of $V-I$ colors from WFPC2 photometry and pseudo-colors measured on Keck spectra

Objects	$V-I$	$m_{4700} - m_{5700}$
n1023-3	0.72	-0.32
n1023-4	0.70	-0.30
n1023-13	1.14	0.11
n1023-14	0.99	-0.09
n1023-16	0.99	0.00
n1023-17	1.01	0.06
n1023-19	1.03	0.05
n1023-21	0.99	0.02
n1023-25	1.24	0.07

Table 4. Brodie & Huchra indices

Object	H β (\AA)	H γ (\AA)	H δ (\AA)	CNR	H+K
n1023-13	0.084 ± 0.007	0.092 ± 0.011	0.030 ± 0.014	0.054 ± 0.011	–
n1023-14	0.123 ± 0.052	0.099 ± 0.076	0.035 ± 0.092	0.080 ± 0.072	0.286 ± 0.123
n1023-16	0.088 ± 0.019	0.099 ± 0.028	0.125 ± 0.037	-0.047 ± 0.025	0.237 ± 0.050
n1023-17	0.148 ± 0.034	0.164 ± 0.059	0.016 ± 0.069	-0.025 ± 0.051	–
n1023-19	0.003 ± 0.037	0.071 ± 0.056	0.164 ± 0.075	-0.119 ± 0.047	0.267 ± 0.105
n1023-21	0.100 ± 0.017	0.087 ± 0.024	0.104 ± 0.029	-0.053 ± 0.020	0.235 ± 0.039
n1023-25	0.183 ± 0.052	0.149 ± 0.081	0.124 ± 0.094	-0.090 ± 0.067	-0.016 ± 0.124

Note. — H γ and H δ are defined as in Brodie & Hanes (1986).

Table 5. Lick/IDS standard star observations

Index	STD	HR3905			HR1805			
		Flux calibr.	Unfluxed	Smoothed	STD	Flux calibr.	Unfluxed	Smoothed
Ca4227	1.820	2.151 ± 0.179	2.179 ± 0.177	1.961 ± 0.098	2.450	3.005 ± 0.284	3.030 ± 0.275	2.680 ± 0.083
G4300	6.870	7.311 ± 0.127	7.415 ± 0.120	6.913 ± 0.061	7.000	7.556 ± 0.212	7.679 ± 0.220	6.859 ± 0.113
hbeta	1.250	1.467 ± 0.064	1.453 ± 0.064	1.337 ± 0.060	0.850	1.411 ± 0.364	1.397 ± 0.363	1.312 ± 0.310
MgB	4.290	4.518 ± 0.032	4.524 ± 0.032	4.416 ± 0.029	3.880	4.097 ± 0.048	4.104 ± 0.050	3.964 ± 0.066
Fe5270	4.130	4.577 ± 0.047	4.580 ± 0.047	4.231 ± 0.041	4.340	4.906 ± 0.092	4.908 ± 0.093	4.586 ± 0.007
Fe5335	3.750	4.519 ± 0.098	4.516 ± 0.097	3.979 ± 0.103	3.910	4.623 ± 0.180	4.622 ± 0.179	4.080 ± 0.131
Mg1	0.172	0.168 ± 0.001	0.163 ± 0.002	0.164 ± 0.001	0.214	0.199 ± 0.005	0.196 ± 0.005	0.194 ± 0.005
Mg2	0.327	0.320 ± 0.001	0.315 ± 0.001	0.316 ± 0.001	0.361	0.347 ± 0.002	0.344 ± 0.002	0.343 ± 0.002

Table 6. Various Lick / IDS indices.

Object	H β (Å)	G4300 (Å)	Ca4227 (Å)	Fe5270 (Å)	Fe5335 (Å)	Mg2 (mag)	CN2 (mag)
n1023-3	7.065 ± 0.380	-1.469 ± 0.535	0.488 ± 0.270	0.369 ± 0.463	0.480 ± 0.574	0.054 ± 0.011	-0.161 ± 0.014
n1023-4	6.120 ± 0.305	-1.242 ± 0.415	-0.014 ± 0.211	0.803 ± 0.354	0.836 ± 0.438	0.035 ± 0.008	-0.135 ± 0.011
n1023-13	1.893 ± 0.164	4.222 ± 0.329	1.017 ± 0.192	2.198 ± 0.174	2.007 ± 0.207	0.096 ± 0.004	0.079 ± 0.012
n1023-14	2.538 ± 1.201	2.587 ± 2.076	0.090 ± 1.265	2.392 ± 1.328	0.683 ± 1.691	0.127 ± 0.035	0.068 ± 0.075
n1023-16	2.070 ± 0.462	2.742 ± 0.820	0.866 ± 0.451	1.641 ± 0.505	1.452 ± 0.625	0.106 ± 0.013	-0.030 ± 0.026
n1023-17	3.461 ± 0.766	0.697 ± 1.732	1.056 ± 0.940	2.057 ± 0.799	1.667 ± 0.985	0.089 ± 0.020	-0.009 ± 0.054
n1023-19	0.467 ± 0.937	1.179 ± 1.764	1.444 ± 0.909	0.313 ± 0.972	-1.096 ± 1.212	0.107 ± 0.025	-0.036 ± 0.050
n1023-21	2.321 ± 0.410	2.294 ± 0.676	0.716 ± 0.371	1.264 ± 0.453	1.252 ± 0.556	0.017 ± 0.011	-0.030 ± 0.021
n1023-25	4.323 ± 1.128	2.874 ± 2.416	-0.528 ± 1.391	3.219 ± 1.179	3.583 ± 1.415	0.143 ± 0.032	-0.064 ± 0.072
Avg	2.125 ± 0.400	2.287 ± 0.510	0.865 ± 0.184	1.644 ± 0.314	0.994 ± 0.455	0.090 ± 0.016	0.007 ± 0.021

Note. — Avg: Average of clusters n1023-13, n1023-14, n1023-16, n1023-17, n1023-19 and n1023-21